Tandem demodulation lock-in amplifier based on digital signal processor for dual-modulated spectroscopy

Jianhuan Qin, Zhiming Huang, Yujian Ge, Yun Hou, and Junhao Chu

Citation: Review of Scientific Instruments **80**, 033112 (2009); doi: 10.1063/1.3098948
View online: https://doi.org/10.1063/1.3098948
View Table of Contents: http://aip.scitation.org/toc/rsi/80/3
Published by the American Institute of Physics

Tandem demodulation lock-in amplifier based on digital signal processor for dual-modulated spectroscopy

Jianhuan Qin,[a] Zhiming Huang, Yujian Ge, Yun Hou, and Junhao Chu
National Laboratory for Infrared Physics, Shanghai Institute of Technical Physics, Chinese Academy of Sciences, Shanghai 200083, People's Republic of China

(Received 18 January 2009; accepted 22 February 2009; published online 25 March 2009)

Dual-modulated spectroscopy is one of the most powerful methods in the measurement of modulation spectroscopy. Here we develop a tandem lock-in amplifier (LIA) based on digital signal processor to implement a novel algorithm of tandem demodulation. The theoretical analysis of demodulation algorithm is presented, and the implementation of this tandem LIA is described in detail. Compared to the traditional demodulating way with two LIAs in cascade, this tandem LIA eliminates the extra quantization error of redundant analog-to-digital and digital-to-analog conversions and removes the limitation to the time constant in the commercial LIA, hence lowers the requirement of frequency ratio in dual-modulated spectroscopy. The applications are given as examples in the photoreflectance (PR) measurements of GaAs (100) thin film and GaSb bulk material, respectively, at the different optical energy regions. The experimental results indicate that this tandem is well capable of PR spectra measurement with good PR lineshapes and reasonable signal noise ratio. A brief comparison of GaAs PR results between tandem LIA and two LIAs is made to prove the efficiency and advantages of the tandem LIA. © *2009 American Institute of Physics.* [DOI: 10.1063/1.3098948]

I. INTRODUCTION

As a powerful tool of detecting weak signal, the lock-in amplifier (LIA) is widely employed in research and development measurement. It works as a very narrow-band filter and theoretically only one Fourier component of system respond can be achieved. A reference signal with the same frequency as measurement signal is required synchronously when the LIA generates the phase and magnitude changes in measurement signal.[1]

Originally, traditional LIAs are set up by analog electronic devices with high performance for most of applications. However, with the gradually increasing requirement of complicated and accurate measurement and the great improvement of the performance of digital system, the replacement of analog instrumentation with a digital one is more and more frequent. The digital LIA with embedded digital signal processor (DSP) can avoid harmonic distortion and thermal shift arising in the analog device, accomplishing considerably better stability.[2] Furthermore, in addition to the well known DSP characteristics of high-speed calculation, easy development and debugging of digital procedure, digital LIA based on DSP can carry out complicated performances and applications.[3]

For different and particular needs, a series of implementations of special digital LIAs with specific algorithm are developed and reported: multiple-channel digital LIA with ppm resolution, multiple-frequency sweeping simultaneously digital LIA, 320-channel dual phase lock-in optical spectrometer, and so on.[4–6] However, none of them consider systems which can measure the weak signal with more than one carrier frequencies synchronously. In order to characterize these kinds of systems, the digital LIA based on DSP capable of tandem demodulating measurement is presented in this work.

Our need for designing and implementing a tandem demodulation LIA arose from dual-modulated spectroscopy application. Traditional modulated spectroscopy for photoreflectance (PR) and electroreflectance encounters significant errors induced by laser scattering disturbance and electromagnetic interference, respectively.[7] To eliminate the noise aforementioned, another amplitude modulation is introduced to form dual-modulated spectrometer. Two standard LIAs connected in series could likely measure detector signal with two different modulation frequencies, high frequency (HF) and low frequency (LF), as first LIA is operated at HF with the analog output connected to the signal input of the second one. However, besides the high cost of commercial digital LIAs, the measurement with two LIAs experiences rather tough limitation to the choice of integral time constant, which conduces that first-step demodulation at HF breaks easily the periodic property of the LF signal. Moreover, redundant analog-to-digital (AD) and digital-to-analog (DA) conversions between LIAs processing induce extra quantization distortion, and different gain and phase stability between LIAs results in more signal error and lower accuracy. Thus, the measurement with two standard LIAs requires higher HF/LF ratio to ensure more accurate measurement. According to the dual modulation principle, the HF is at least ten times larger than the LF to avoid the signal confusion.[8] How-

[a]Electronic mail: qinjianhuan@gmail.com.

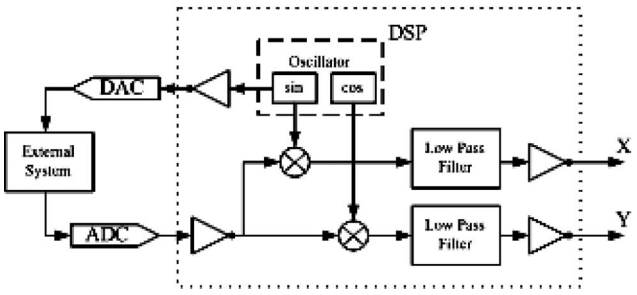

FIG. 1. Basic LIA diagram.

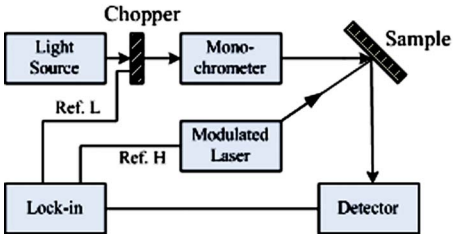

FIG. 2. (Color online) Schematic diagram of dual-modulated PR spectrometer.

ever, for the two LIAs in cascade system, this ratio amount HF/LF has to raise as large as around 40 to achieve good measurement results.

Considering the deficiency in the system with two LIAs in series, we develop a novel digital LIA with the help with powerful DSP device to realize tandem demodulation for the dual-modulated spectroscopy application instead of two standard LIAs, which can be characterized as "tandem LIA." The implementation of this LIA allows us to achieve much improvement: the strong capability of high-speed calculation of DSP can afford twice correlative demodulation in a very short time, reducing total measurement time; during the whole signal processing procedure, only one AD converting is required, and then twice demodulating calculations are carried out with digital data in memory, avoiding the quantization distortion induced by redundant AD and DA conversions; with the integrated clock generator controlled by DSP, we are able to produce two modulation frequency signal of the same original phase, which help to keep well the signal periodic property during the tandem demodulation.

In this article, first we introduce the basic principle of digital LIA. Then a description of how new tandem demodulating LIA works is presented. Theoretical analysis indicates that the proposed LIA can fully carry out the measurement of signal with two modulation frequencies, hence it can be applied in the dual-modulated spectroscopy. The implementation of this novel LIA is given in detail. Some representative experimental results are shown to prove the efficiency and advantage of tandem demodulation LIA in dual-modulated measurement. A brief discussion is made and a conclusion is reached finally.

II. BASIC DIGITAL LIA

The digital LIA composed of four parts: AD and dc converters, digital multiplier stages, digital oscillator, and low-pass filters, as shown in Fig. 1.[8] The measurement principle of LIA carries out a correlative demodulation with the same reference frequency as the carrier signal. The oscillator generates the same measurement and reference sinusoidal signals. The measurement signal goes through external system that produces modification of the signal phase and magnitude and then is collected into LIA by AD converter. The input signal is multiplied by the in-phase reference signal and the in-quadrature (90° shifted) reference signal in the multiplier stages, respectively. The low-pass filters cut off the ac signal and only keep the dc components. With both of measurements in-phase (X) and in-quadrature (Y), the magnitude and phase of the measurement signal with respect to the reference can be computed and recorded.

To reduce the noise in the low-pass filters, it is required to have very low cut-off frequency. However, lower cut-off frequency represents larger integral time constant, which makes the response of LIA slower. A convenient trade-off between noise level and measurement speed should be made for each experiment.

III. WORK PRINCIPLE ANALYSIS

This digital LIA performs tandem demodulation and works as two LIAs connected in cascade. However, only one single analog channel for input and one single analog channel for output are required for measurement, and all the calculations and operations are implemented in a lock-in module based on DSP. So we can characterize this LIA as an integrated tandem LIA, which avoids the quantization noise introduced by redundant AD conversions, and reduces the total measurement time.

The system of PR measurement is taken as an example to indicate how this tandem LIA works. As shown in Fig. 2, the LIA generates two reference signals with the zero original phases, Ref. L and Ref. H at f_L (LF) and f_H (HF) to drive the chopper and the modulated laser, respectively. To obtain more accurate measurement result, we usually set the two modulation frequency as $f_H \geq 20 f_L$. The signal collected by detector can be described as follows:[9]

$$S(\lambda)_{\mathrm{ac}} = B(\lambda)K_d(\lambda)\Delta R(\lambda)\sin(\omega_L t + \theta_L)\sin(\omega_H + \theta_H) + I_p(\lambda_p)K_d(\lambda_p)\sin(\omega_H + \theta_p) + I_l(\lambda_l)K_d(\lambda_l)\sin(\omega_H + \theta_l),$$

where $\omega_L = 2\pi f_L$ and $\omega_H = 2\pi f_H$, $S(\lambda)_{\mathrm{ac}}$ is the ac output signal of the photodetector as a function of wavelength λ. $B(\lambda)$ is the intensity of the narrow-band probe beam around wavelength λ. $K_d(\lambda)$ represents the detector respond and possibly contains optical path factor. $\Delta R(\lambda)$ is modulated reflectance of the sample illuminated synchronously by modulated laser and probe beam from light source. $I_p(\lambda_p)$ and $I_l(\lambda_l)$ are, respectively, modulated laser induced photoluminescence and scattered laser light.

After the first-step demodulation with a reference signal $\sin(\omega_H t)$, stochastic noise is eliminated and $S(\lambda)_{\mathrm{ac}}$ evolves to S_1^{LIA},

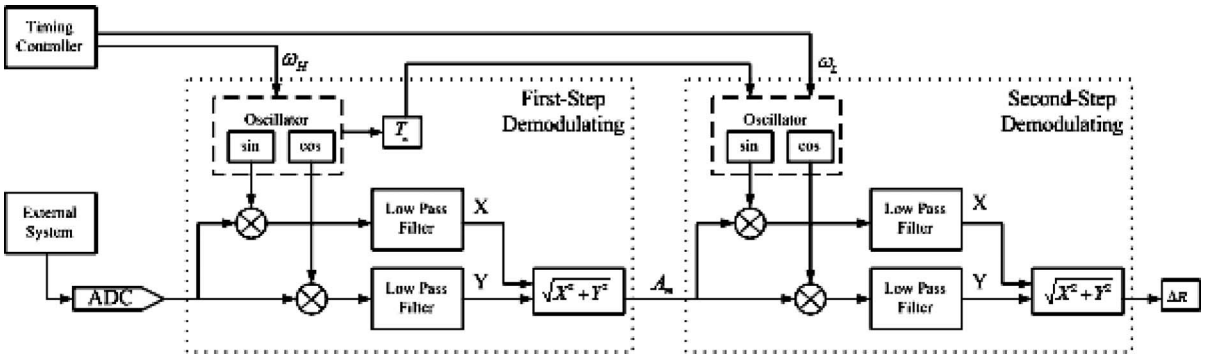

FIG. 3. Schematic diagram of tandem demodulation processing in this tandem LIA.

$$S_1^{\mathrm{LIA}} = \frac{K_1^{\mathrm{LIA}}}{2}[B(\lambda)K_d(\lambda)\Delta R(\lambda)\sin(\omega_L t + \theta_L) + I_p(\lambda_p)K_d(\lambda_p) + I_l(\lambda_l)K_d(\lambda_l)],$$

where K_1^{LIA} is the transfer function of first-step demodulation, which can be considered as a constant. After second-step demodulation with a reference signal $\sin(\omega_L t)$, final output of LIA S_2^{LIA} is approached,

$$S_2^{\mathrm{LIA}} = \frac{K_2^{\mathrm{LIA}} K_1^{\mathrm{LIA}} B(\lambda)K_d(\lambda)}{4}\Delta R(\lambda),$$

where K_2^{LIA} is the transfer function of second-step demodulation, similarly a constant. Clearly, two steps of demodulation remove the unwanted spurious signals, leaving the modulated reflectance ΔR.

For the disadvantages discussed above, the system of two LIAs in series need a high ratio HF/LF and long measurement time to perform a tandem demodulation. In this LIA, a novel algorithm is established to carry out the tandem demodulation, as illustrated in Fig. 3. Assume $f_H = Nf_L (N > 20)$, where N is an integer, and both of modulating signals start with a zero original phase. In this case, one period of LF signal comprises N complete HF cycles.

In the first stage, the correlative demodulation of high-frequency modulating signal is executed. As the integral time constant T_1^{LIA} is exactly defined to N_1 HF periods ($T_1^{\mathrm{LIA}} = N_1/f_H$, N_1 and N/N_1 are both integers). Every N_1 periods of HF signal convert to an amplitude value A_m by first-step correlative demodulation. The discrete amplitude sequences $A_m (m = 1, 2, \ldots, N/N_1)$ recover a complete cycle of the LF signal. Meanwhile, the time positions T_m corresponding to amplitude elements A_m are recorded to produce synchronous reference signal for the second-step demodulation,

$$T_m = \left(m - \tfrac{1}{2}\right)\frac{2\pi N_1}{\omega_H}, \quad \left(m = 1, 2, \ldots, \frac{N}{N_1}\right).$$

In the second demodulating stage, a reference sequence with frequency f_L is generated according to the time sequence T_m,

$$R_m^{\sin} = \sin(\omega_L T_m), \quad R_m^{\cos} = \cos(\omega_L T_m), \quad \left(m = 1, 2, \ldots, \frac{N}{N_1}\right).$$

With the amplitude A_m and reference signal $R_m^{\sin}$ and $R_m^{\cos}$ sequences, we can remove the LF modulating signal by correlative demodulating once more, and extract expecting signal finally.

From the lock-in principle above, it is clear that new tandem demodulating algorithm keeps well the periodic property between two processing stages, and gets rid of limitation to the time constant in the traditional way. Furthermore, all the demodulating procedures are operated in digital format based on DSP, removing the quantization error derived by extra AD and DA conversions. With the powerful capability of DSP computation, two demodulating stages are operated in parallel to reduce whole experimental time.

IV. TANDEM DEMODULATION LIA IMPLEMENTATION

A low-cost lock-in circuit board based on DSP (TMS320C6701) has been designed for the implementation of tandem demodulation, which comprises three core functional modules as follows.

A. Main processor: TI TMS320C6701 DSP

The main processor adopts a 32-bit floating-point DSP (TMS320C6701) (Ref. 10) running at 167 MHz clock rate with high performance of up to 1 giga floating-point operations per second, which support real-time processing and complicated calculation. 1 mbit on-chip static random access memory is available, involving 512 kbit internal program storage where the lock-in instructions resides and 512 kbit dual-access internal data memory space. 1 Mbit × 32 bit external synchronous dynamic random access memory is connected to DSP by the external memory interface to meet the requirement of high-speed storage of vast measuring data for tandem LIA.

B. Timing controller: Xilinx Spartan-3A FPGA XC3S400

A high performance-price field-programmable gate array FPGA (XC3S400) (Ref. 11) running at 50 MHz global clock is used as timing controller to manage two-channel modulating signals. Quite a low delay time (down to several nanoseconds) guarantees high accuracy of modulating signal frequency and phase. Furthermore, with up to 502 input/output (I/O) pins, it extends considerably I/O resources for DSP peripheral circuit management.

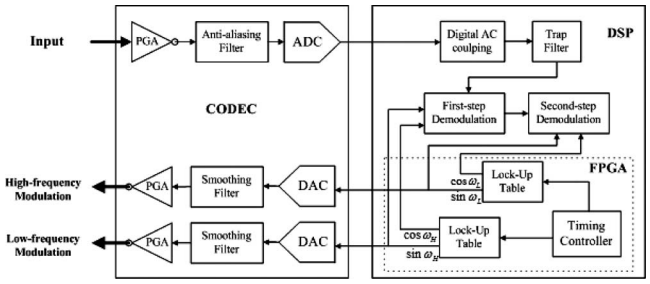

FIG. 4. Functional architecture of tandem LIA. Three block diagrams represent operations of DSP, CODEC, and FPGA, respectively.

C. Audio codec (CODEC4231A)

One on-chip CODEC4231A, connected to DSP through multichannel buffered serial ports contains two 16-bit analog-to-digital converters (ADCs) and two 16-bit digital-to-analog converters (DACs) with a programmable sample rate from 5.5125 to 48 kHz, a programmable gain amplifier and an antialiasing filter for input, and one smoothing filter for the output.

The sampling rate f_S is an important parameter for LIA performance. According to the Nyquist theorem, the maximum frequency f_M present in the signal must be below $f_S/2$. However, for the lock-in system, a large number of simulations and experiments indicates that, when $f_S/f_M<16$, much longer integral time constant should be taken to achieve the satisfying result. When $f_S/f_M>32$, little improvement in measurement accuracy can be obtained. The proper sampling rate chosen is recommended as $M=f_S/f_M\in[16,32]$ and M is an integer, which makes the relative error in measurement lower than 3% even when signal signal-noise-ratio (SNR)$=-126$ dB in a strongly noisy background.

The tandem LIA processing architecture is presented in Fig. 4. As all the experimental parameters are ready, the DSP tandem lock-in performs the following operations:

(1) DSP internally initializes all the measurement parameters, involving sampling rate, high and low modulating frequencies, digital filters coefficients, as well as time constants in two-stage demodulations, and then sends the corresponding control instructions to configure onboard CODEC and FPGA.
(2) FPGA boots with DSP trigger signal and works as a timing controller to generate two-channel modulating signals for external modulation drivers. Meanwhile, the synchronous digit reference signals in-phase and in-quadrature (sine and cosine) are fed back to DSP for internally demodulating computation.
(3) External signals are collected into DSP by CODEC converter, and one trap filter and one ac coupling filter accomplished the preprocessing operations.
(4) First-step demodulation is carried out by multiplying the input digital signal with high-frequency references and filtering ac components of calculated products using low-pass filter. Every N_1 period of HF signal converts to one dc amplitude value, and relevant time location is recorded for LF demodulating process.
(5) Second-step demodulation for LF carrier signal is implemented with discrete amplitude values from the first step multiplied with reference signals defined by the time sequence recorded in the first step. A low-pass filter with very low cut-off frequency is applied to the computation products to keep the resulting dc signal which represents final measurement outcome.

The digitally controlled reference signal is the most critical component of the development because the whole lock-in instrument performance depends on this stage. Here we employ the technique of direct digital synthesis (DDS) to accomplish the requirement of short computing time and dynamic frequency synthesis.[12] A sine lookup table with 128 $\times$32-bit float elements is established in FPGA embedded BlockRAM. Combined with linearly interpolating the intermediate values, this type of digital oscillator produces a complete-cycle sine wave form that is almost free of total harmonic distortion (THD). The approximate estimate of the maximal THD is less than -210 dB in computer simulation. The cosine synthesis can be obtained by keeping 90° phase difference from sine value.

The phase accumulator plays a significant role in DDS. To enhance system processing speed, four 8-bit accumulators in series perform as one 32-bit accumulator, instead of the ready-made 32-bit counter module in FPGA. The simulation proves that such a pipeline accumulator shortens the delay time and makes DDS afford for higher frequency synthesis. The phase accumulator is actually functioning as an address counter that increments its stored amount according to the required output frequency each time (20 ns at 50 MHz) it receives a clock pulse. This address counter steps through and accesses each lock-up table location and corresponding content with equivalent sine amplitude word is presented to CODEC DAC. The high-speed DAC and smoothing filter recover an analog sine wave in response to digital values from lock-up table. In order to get the tunable sine wave frequency, we just need to change the increment in the phase accumulator. Two phase accumulators with different increment numbers are utilized to provide high-frequency and low-frequency analog modulating signals for external modulating drivers, respectively. Besides, two synchronous digital reference clocks at high and low frequencies are supplied to meet the need of digit-control modulators. According to DDS principle, with a 32-bit counter and 50 MHz reference clock (FPGA global clock), we can get frequency-tunable sine waves with frequency resolution 0.0116 Hz. By using the frequency divider to reduce the reference clock, lower frequency resolution can be achieved.

Once the external signal with two modulation frequencies, f_H and f_L ($f_H=Nf_L, N\geq 20$), passes through the system, a programmable gain amplifier (PGA) applies to adjust the signal level appropriate to the experiment.

After the codec ADC converts the analog input signal to digital at designated sampling rate, a digit ac coupling network composed of a digital resistance/capacitance performs as a first-order high-pass filter with a 0.1 Hz cut-off frequency to remove the dc component of input signal, which counts for little in the measurement.

The interfering signal at the power frequency must be eliminated in weak-signal detection. Hereby we exploit a

trap filter to clear up the disturbance of power noise. The transfer function of trap filter is designed with mirror symmetry as the following:

$$H(z^{-1}) = \frac{1 + az^{-1} + z^{-2}}{1 + apz^{-1} + p^2 z^{-2}}$$

where p is a constant coefficient close to one but less than one, which determines the bandwidth and attenuation of trap filter. At the designated sampling rate f_S, the coefficient a chooses the center frequency in the trap filter as $f_0 = \arccos(-a/2)/2\pi f_S$. With given f_0 and f_S, the coefficient of trap filter, a and p, can be calculated and modified to accomplish specific trap bandwidth and depth. Here we set the center frequency $f_0 = 50$ Hz (power frequency), and the trap depth reaches -114 dB, which almost completely eliminates the power disturbing signal.

In the stage of first-step demodulation, the essential operation of the demodulator DSP is to multiply the digitized input signal by the in-phase and in-quadrature reference sequences, and then to operate on the results with digital low-pass filters. The in-phase reference signal comes directly from internal sine look-up table, and the in-quadrature reference is derived with a 90° shift in the index of sine look-up table ($128/4 = 32$ elements). The finite impulse response (FIR) filter holding a linear phase response is contrived to realize a high-performance low-pass filter with a cut-off frequency $f_C/f_S = 0.005$ (240 Hz at 48 Ksps). The FIR filters offer a substantial advantage in response time compared with analog filters and digital infinite impulse response filters. One Blackman window function is introduced to make the stop-band attenuation down to -120 dB. The output amplitude and corresponding time location sequences are sent to next demodulating stage every N_1 HF periods (nominal time constant).

In the second-step demodulation, the amplitudes generated by the first step are multiplied by the reference sequences computed by the time location values from the first step. Also, the same low-pass FIR filter as mentioned in first-step demodulation applies to extract the dc component, which represents ultimate measurement result. As the computing operations in first-step demodulation reduce sampling rate in second stage down to Nf_L/N_1, the cut-off frequency of the low-pass filter in second-step demodulation can decrease to 10 Hz as $N = 20N_1$, $f_L = 100$ Hz. The final results are stocked in the on-chip memory and synchronously sent to the on-board liquid crystal display for on-time display.

V. EXPERIMENTAL ANALYSIS

To evaluate the performance of this tandem LIA, the PR spectrum measurements are carried out for the GaAs and GaSb samples. The experimental configuration is schematically illustrated in Fig. 2. The tandem LIA supplies two-channel modulation signals at HF f_H and LF f_L, respectively, to drive the pump laser and mechanical chopper applied to the probe beam from tungsten lamp. The monochrometer MS257™ Model 77 700A is employed to implement wavelength scanning at designated range. The signal collected by the detector is sent into the LIA and the tandem demodulation procedure is accomplished in the LIA to generate the PR spectrum value.

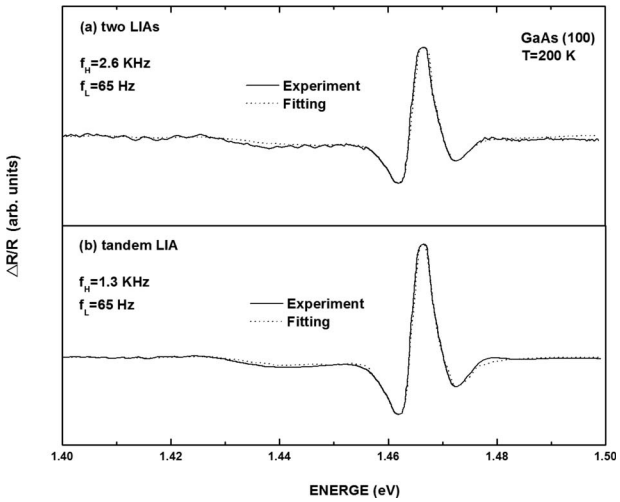

FIG. 5. PR spectra (real lines) and their least-square curve fitting (dashes) of GaAs (100) at 200 K measured by (a) two LIAs with $f_L = 65$ Hz, $f_H = 40$, $f_L = 2.6$ kHz, and (b) tandem LIA with $f_L = 65$ Hz, $f_H = 20$, $f_L = 1.3$ kHz.

First, the PR spectra measurements on the GaAs (100) sample at 200 K are performed by using this tandem LIA and two SR Model 7265 LIAs in series, respectively, as shown in Fig. 5. The tandem LIA sets the two modulating frequencies as $f_L = 65$ Hz, $f_H = 20F_L = 1.3$ kHz. For two LIAs in series, in order to get the comparably good measurement results, however, we have to set the high frequency as $f_H = 40f_L = 2.6$ kHz, which is twice as large as that in the tandem LIA. The time constants for the tandem LIA and two LIAs system take the values of 155 and 200 ms, respectively. Both the experimental curves measured by the tandem LIA [Fig. 5(b)] and two LIAs [Fig. 5(a)] give good descriptions of complete derivative line shape features for PR spectra, and show definite and strong peaks in the spectral region of 1.455–1.475 eV, which is consistent with the GaAs fundamental bandgap 1.465 eV at 200 K. In contrast with the spectra established by two LIAs, it is clear that the tandem LIA produces much smoother experimental curve with higher SNR even under lower modulating HF. Here the SNR is calculated with the ratio of the maximum peak value to the maximum background noise. As illustrated in Fig. 5, the SNR of two LIAs measurement (a) is about 20, while the SNR in tandem LIA measurement (b) reaches up to 31.

To check the characteristics of the PR spectrum, we take a curve fitting with a line shape function of third derivative for a low electrical field modulation and unbound situation as following:

$$\frac{\Delta R}{R} = \mathrm{Re}\sum_i C_i e^{j\theta_i}(E - E_i + j\Gamma_i)^{-n},$$

where Re represents the real part, and C_i and θ_i are the amplitude and phase factor of the ith line shape. E_i and Γ_i express the energy and corresponding broadening parameter of the ith transition. n relies on the parabolic critical point model. Here it takes a value of $n = 2.5$ for three-dimensional critical point type. The fitting curves are presented as the

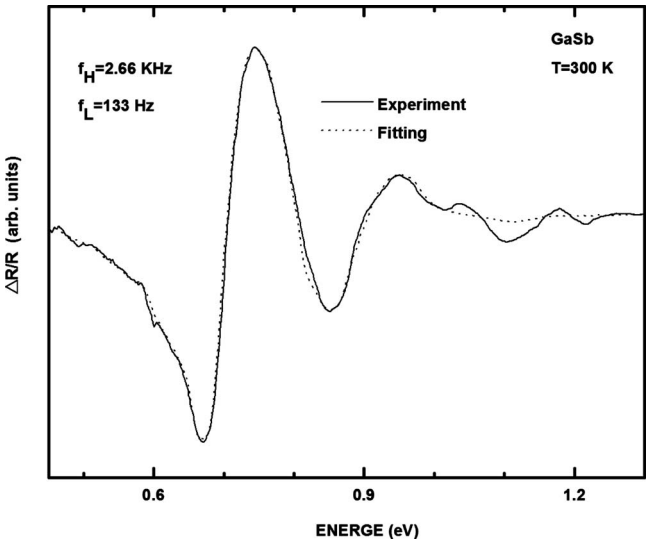

FIG. 6. PR spectra (real) and its least-square curve fitting (dashes) of GaSb at room temperature measured by tandem LIA with f_L=133 Hz, f_H=20, f_L=2.66 kHz.

dotted lines in Fig. 5, which provide a good match for the experimental curves and hence manifest well the third derivative properties of PR spectrum. The normalized standard deviation σ_n is chosen as a comment of measurement goodness,

$$\sigma_N^2 = \frac{\sum_i (E_i - F_i)^2}{\sum_i E_i^2}$$

where E_i and F_i are experimental and fitting data, respectively.

The normalized standard deviations are calculated for Fig. 5 as σ_N=0.204 for two LIAs and σ_N=0.091 for tandem LIA, respectively. It is obviously indicated that the tandem LIA gives a better measurement result than two LIAs in series.

Another sample GaSb bulk is chosen to inspect the performance of this tandem LIA at smaller optical energy region, which has the fundamental bandgap 0.703 eV at room temperature 300 K. As the background noise increases with the wavelength rising, the LF f_L for modulating probe beam is set as large as 133 Hz to eliminate the effect of background noise. Correspondingly, the high-frequency f_H for laser pumping turns to 2.66 kHz to maintain the relationship f_H=20f_L in the tandem LIA and the time constant is chosen as 300 ms. In the two LIAs system, the high modulating frequency should be set as f_H=40f_L=4.32 kHz, as discussed in the measurement of GaAs. However, for the limitation to maximum frequency of the chopper at 4 kHz, the measuring way with two LIAs in cascade cannot take effect in this case. Figure 6 illustrates the PR curve of GaSb recorded by the tandem LIA, which depicts well the derivative characteristics of PR spectrum with obvious peaks at 0.65–0.85 eV. The third derivative fitting result is also shown as dotted line shape. The SNR of experimental data is about 29 and σ_N =0.154 for the fitting data. Both the experimental data and fitting data indicate that the tandem LIA functions well with a reasonable SNR in the PR measurement at low energy range 0.4–1.3 eV, while the two LIA systems cannot perform the measurement.

VI. DISCUSSION

A lot of experimental systems have been developed to improve the measurement for the modulated spectroscopy, one of which is dual modulation with two modulating carried frequencies and two LIAs. However, because of the limitation related with the integral time constant and multiple AD conversions, the two LIAs in series cannot perform well in the demodulation of two modulated frequencies at the low HF/LF ratio. Here we develop a tandem LIA based on DSP to carry out the tandem demodulation, which generates two-channel modulating signals with adjustable frequency and programmable original phase, and operates two steps of demodulation in the digital domain after once AD converting. Besides, the flexible configuration of time constant in the lock-in stages helps to optimize the demodulation processing.

The comparison of GaAs PR measurements between two LIAs and tandem LIA indicates that the tandem LIA presents better SNR (about 31) and smoother experimental curve than two LIAs even at lower frequency ratio (HF/LF=20). Better data fitting can be accomplished for the results of the tandem LIA with third derivative model. Moreover, the tandem LIA applies to the small energy range down to 0.4 eV for PR spectra of GaSb with a SNR of around 29, while the two LIAs system fail to perform the measurement as the requirement of high HF/LF ratio (40) exceeds the maximum work frequency of the mechanic chopper. Both of GaAs and GaSb PR spectra measured by the tandem LIA show good properties of third derivative line shape with strong peaks at 1.455–1.475 eV for GaAs and 0.65–0.85 eV for GaSb, respectively, which match the theoretic bandgap values well.

To sum up this tandem LIA, a novel algorithm of tandem demodulation is established, and is implemented by a low-cost circuit board based on DSP computational unit and FPGA DDS unit. The tandem LIA eliminates the shortages of time constant limitation and quantization error induced by the cascaded AD and DA conversion in the traditional two LIAs system. The experimental results manifest its positive function on the PR measurement at visible and near infrared wavelength regions. With the help of higher frequency modulation drivers, the higher HF/LF ratio is available and the application of this tandem LIA can be extended to the mid-infrared or longer wavelength on PR spectroscopy.

ACKNOWLEDGMENTS

This work was supported by NSF (Grant Nos. 60707022 and 60527005), National Grant Foundation Project (Grant Nos. 2007CB924901), and CAS (Grant Nos. YZ200835 and C2-39).

[1] J. Gaspar, S. F. Chen, A. Gordillo, M. Hepp, P. Ferreyra, and C. Marques, Microprocess. Microsy. **28**, 157 (2004).
[2] S. C. Gupta, Proc. IEEE **63**, 291 (1975).
[3] F. Barone, E. Calloni, L. DiFiore, A. Grado, L. Milano, and G. Russo, Rev. Sci. Instrum. **66**, 3697 (1995).

[4] P. Probst and A. Jaquier, Rev. Sci. Instrum. **65**, 747 (1994).
[5] M. O. Sonnaillon and F. J. Bonetto, Rev. Sci. Instrum. **76**, 024703 (2005).
[6] P. S. Fodor, S. Rothenberger, and J. Jevy, Rev. Sci. Instrum. **76**, 013103 (2005).
[7] F. H. Pollak and H. Shen, Mater. Sci. Eng. R. **10**, 275 (1993).
[8] Signal Recovery, Model 7265 DSP Lock-in Amplifier Instruction Manual 2005 (http://www.signalrecovery.com).
[9] H. Shen, P. Parayanthal, Y. F. Liu, and F. H. Pollak, Rev. Sci. Instrum. **58**, 1429 (1987).
[10] Texas Instruments, TMS320C6701 Floating-Point Digital Signal Processor 2004 (http://www.ti.com)
[11] Xilinx, Spartan-3A FPGA Family: Data Sheet 2007 (http://www.xilinx.com)
[12] Analog Devices Inc., A technical tutorial on Direct Digital Synthesis 1999 (http://www.analog.com)